

1 Polar Confinement of Saturn's Magnetosphere 2 Revealed by in-situ Cassini Observations

N. M. Pilkington,^{1,2} N. Achilleos,^{1,2,3} C. S. Arridge,^{4,2} A. Masters,³ N.

Sergis,⁵ A. J. Coates,^{4,2} and M. K. Dougherty⁶

arXiv:1401.2445v1 [astro-ph.EP] 10 Jan 2014

Corresponding author: N. M. Pilkington, Department of Physics and Astronomy, University College London, Gower St., London, WC1E 6BT, UK. (nathanp@star.ucl.ac.uk)

¹Department of Physics and Astronomy,

Abstract. Plasma rotation plays a large role in determining the size and shape of Saturn's disc-like magnetosphere. A magnetosphere more confined to the equator in the polar regions is expected as a result of the interaction between this type of obstacle and the solar wind. In addition, at times away from equinox, a north-south asymmetry is expected where the magnetopause

University College London, Gower St.,
London, WC1E 6BT, UK.

²Atmospheric Physics Laboratory, The
Centre for Planetary Sciences at
UCL/Birkbeck, Gower St., London, WC1E
6BT, UK.

³Institute of Space and Astronautical
Science, Japan Aerospace Exploration
Agency, Sagamihara, Kanagawa, Japan.

⁴Mullard Space Science Laboratory,
Department of Space and Climate Physics,
University College London, Dorking, UK.

⁵Academy of Athens, Office of Space
Research & Technology, Athens, Greece.

⁶Blackett Laboratory, Imperial College
London, London, UK.

8 will be further confined in one hemisphere but less confined in the opposite
9 hemisphere. Examining the extent of this confinement has been limited by
10 a lack of high-latitude spacecraft observations. Here, for the first time, di-
11 rect evidence for polar confinement of Saturn’s magnetopause has been ob-
12 served using in-situ data obtained by the *Cassini* spacecraft during a series
13 of high-inclination orbits between 2007 and 2009. Following techniques es-
14 tablished by previous authors, we assume an equilibrium between the solar
15 wind dynamic pressure (which *Cassini* is generally unable to measure directly),
16 and the magnetic plus plasma pressure inside the magnetosphere. This as-
17 sumption thus allows us to estimate the upstream solar wind dynamic pres-
18 sure (D_P) for a series of magnetopause crossings, and hence to determine the
19 expected location and global shape of the magnetopause as a function of D_P .
20 A clear divergence from the familiar axisymmetric models of the magneto-
21 sphere is observed, which may be characterised by an ‘apparent flattening
22 parameter’ of $0.81+0.03/-0.06$ (representing a simple dilation of the nom-
23 inal axisymmetric boundary along the Z_{KSM} axis such that the extent is re-
24 duced by approximately 19% in this direction). This figure is insensitive to
25 variations in D_P .

1. Introduction

26 The solar wind is a supersonic plasma which continuously flows away from the Sun
27 and fills the entire solar system. Its formation was theorised by *Parker* [1958] and it was
28 first directly observed by the Luna 1 spacecraft and confirmed by *Snyder and Neugebauer*
29 [1963] using Mariner 2 observations. It carries with it a remnant of the solar magnetic
30 field, known as the Interplanetary Magnetic Field (IMF). When it encounters a magne-
31 tised body it is slowed, heated and deflected around that obstacle. The resulting cavity,
32 to which the solar wind cannot obtain direct access, is known as the magnetosphere.

33 The magnetopause is the current sheet boundary that separates the plasma populations
34 and magnetic fields of solar and planetary origin and defines the area within which forces
35 internal to the magnetosphere dominate the ram pressure of the solar wind. The solar
36 wind ram, or dynamic, pressure is highly variable and has a strong influence on the mag-
37 netosphere, whose size and shape can exhibit rapid variability.

38 Magnetospheres vary greatly in their global structure depending chiefly on the strength
39 of the planetary magnetic field, the amount of internal plasma and the distance from
40 the Sun. The magnetosphere of Mercury, for example, is relatively small and can barely
41 hold off the solar wind from the planet's surface [e.g., *Slavin et al.*, 2007], whereas the
42 magnetosphere of Jupiter is the largest structure in the solar system [e.g., *Bagenal*, 1992].
43 This is due, in part, to its strong magnetic field and also due to the presence of a highly
44 volcanically active moon, Io, which was found to release approximately 1000 kg s^{-1} of sul-
45 phur dioxide gas into the magnetosphere [e.g., *Dessler*, 1980]. This is then partly ionised,
46 through charge exchange, into a plasma and is picked up by the rotating ambient plasma

47 flow in the vicinity of the moon and acts to significantly inflate the magnetosphere due
48 to enhanced plasma pressure. The solar wind dynamic pressure is also much smaller at
49 Jupiter's orbital distance.

50 In terms of size, the Earth's magnetosphere lies somewhere between the extreme examples
51 previously discussed. It doesn't have a large, internal source of plasma as Jupiter does,
52 but it experiences a much smaller dynamic pressure than Mercury's magnetosphere owing
53 to its larger distance from the Sun. A statistical study by *Achilleos et al.* [2008] found
54 that Saturn's magnetospheric size follows a bimodal distribution (the sum of two Gaus-
55 sian distributions) with the most common stand-off distances at ~ 22 and ~ 27 Saturn
56 planetary radii (R_S). The Kronian magnetosphere thus falls somewhere between Earth
57 and Jupiter in terms of size and exhibits a similar 'dual state' to the Jovian system [*Joy*
58 *et al.*, 2002].

59 Plasma loading plays a significant role in shaping the Kronian magnetosphere and Ence-
60 ladus is the dominant source of plasma in this system. It is thought to be cryovolcanic,
61 its volcanism arising from the tidal heating of its interior by Saturn. *Tokar et al.* [2006]
62 and *Pontius and Hill* [2006] estimate that 100 kg s^{-1} of water molecules are liberated by
63 the moon, *Waite et al.* [2009] found that smaller quantities of carbon dioxide, ammonia
64 and hydrocarbons are also present in the Enceladus plasma. More recent estimates made
65 by *Spencer* [2011] place the mass outflow rate to be as high as 200 kg s^{-1} .

66 The water molecules are then partially ionised and the presence of this outflowing plasma
67 acts to inflate the magnetosphere significantly. The rapid rotation of the planet confines
68 it to the equatorial plane and forms a magnetodisc. It then diffuses into the outer mag-
69 netosphere due to centrifugal instabilities as described by *Kivelson and Southwood* [2005].

70 Only the ions and electrons with sufficient energy can escape and travel along the field
71 lines to higher latitudes.

72 The obstacle presented to the solar wind flow is thus disc-like in nature and is more
73 streamlined than the relatively blunt obstacle presented by the terrestrial magnetosphere.

74 The solar wind flows more easily over the polar regions of a disc-like magnetosphere and
75 thus some degree of polar flattening of the magnetopause is expected.

76 At times when the dipole moment of the planet is tilted with respect to the solar wind
77 flow (i.e. no longer perpendicular), a north-south asymmetry (or 'hinging') in the mag-
78 netosphere is formed. As a result, the magnetosphere may appear further confined in
79 one hemisphere whereas an apparent inflation may be observed in the other hemisphere.

80 The angular separation between the magnetic dipole and the solar wind direction varies
81 seasonally so the magnitude of this effect is also thought to vary with planetary season.

82 It is difficult to distinguish between these sources of confinement, and studies at different
83 planetary season may be the only way to unambiguously separate them.

84 An additional effect is that of the magnetospheric oscillation observed at Saturn by e.g.
85 *Espinosa and Dougherty* [2000, 2001]; *Cowley et al.* [2006]; *Kurth et al.* [2008]; *Andrews*
86 *et al.* [2008]; *Clarke et al.* [2010]; *Arridge et al.* [2011]; *Provan et al.* [2011]; *Andrews et al.*
87 [2012]; *Provan et al.* [2012, 2013]. This oscillation seems to be strongly linked to the phase
88 of the Saturn Kilometric Radiation (SKR) and appears to be caused by a current system
89 which rotates with the planet. It has been suggested by *Espinosa et al.* [2003] that a
90 compressional wave is generated close to the planet by an equatorial magnetic anomaly
91 which causes a periodic change in the magnetic field with a period close to that of the
92 planet's rotation. *Clarke et al.* [2006] observed planetary-period oscillations in the mag-

93 netopause boundary of amplitude 1-2 R_S . As such, it is important to consider the effects
 94 of this anomaly on the structure of the magnetopause and its impact on its high-latitude
 95 structure.

96 Polar flattening of the Jovian magnetosphere was observed by *Huddleston et al.* [1998]
 97 using data from the *Galileo*, *Ulysses*, *Voyagers* 1 and 2 and *Pioneers* 10 and 11. They
 98 concluded that the disk-like shape of the obstacle was the cause of the apparent flattening
 99 along the north-south axis. Similar results were found by *Joy et al.* [2002], who used
 100 a combination of observations made by the same spacecraft and MHD simulations, and
 101 found that the degree of asymmetry varied with solar wind dynamic pressure.

102 *Huddleston et al.* [1998] found a power-law relation between the magnetopause stand-off
 103 distance and the upstream dynamic pressure just as *Shue et al.* [1997] found one for the
 104 terrestrial magnetosphere,

$$r_0 \propto D_P^{-\frac{1}{\alpha}} \quad (1)$$

105 where r_0 is the magnetopause stand-off distance, D_P is the solar wind dynamic pressure
 106 and $\alpha = 6$ for a dipole-like configuration as was found for the Earth by *Shue et al.*
 107 [1997]. *Huddleston et al.* [1998] found a value of α between 4 and 5 for Jupiter, indicating
 108 that the Jovian magnetosphere is more compressible and the magnetopause stand-off
 109 distance reacts more strongly to changes in the dynamic pressure than the terrestrial
 110 magnetosphere.

111 A similar study for the Kronian magnetosphere was made by *Arridge et al.* [2006] and is
 112 the basis of the current study. They used boundary crossings from the first six orbits of
 113 *Cassini* to build a shape model of the equatorial magnetosphere and investigate how the
 114 size of the magnetosphere reacts to changes in the solar wind dynamic pressure. They

115 found that the size of the magnetosphere could also be described by a power law. A
116 characteristic value of α close to that previously found for Jupiter of 4.3 ± 0.4 was found.
117 A similar study made by *Achilleos et al.* [2008] found a value of 5.17 ± 0.30 .
118 *Kanani et al.* [2010] built upon this by using a model that included the plasma pressure
119 contributions of electrons and suprathermal ions and also used a more realistic expression
120 for the thermal solar wind pressure. They found a value of α of 5.0 ± 0.8 . This implies an
121 intermediate compressibility between that of the Jovian and the terrestrial magnetosphere,
122 and this has also been confirmed by *Jia et al.* [2012] using a global MHD simulation of
123 the Kronian magnetosphere.

124 This study extends this previous work to the high-latitude magnetosphere. Previous
125 studies of Saturn's magnetopause have involved near-equatorial spacecraft orbits only
126 and, hence, have been unable to make any direct assessment of the extent of its polar
127 flattening. As such, the work presented herein represents the most complete picture of
128 Saturn's magnetosphere to date.

129 In Section 2 we discuss the model used to undertake this study and in Section 3 the data
130 used to find the boundary crossings to which the new model is fitted. The results of
131 fitting the new model to the data are reported in Section 4 and in Section 4.7 we consider
132 the phase of Saturn's global magnetic oscillation at each point that the spacecraft crosses
133 the magnetosphere in order to determine whether this could be the cause of the observed
134 confinement. Finally, the results of this study are discussed and conclusions are drawn in
135 Section 5.

2. The model

2.1. Previous work

136 This study builds on the work of *Arridge et al.* [2006] and *Kanani et al.* [2010] who mod-
 137 elled the magnetopause of Saturn by assuming pressure balance between the solar wind
 138 dynamic pressure and the magnetic pressure at the magnetopause boundary. In reality,
 139 the magnetopause is unlikely to ever be in true equilibrium, but when considering the
 140 average behaviour of the magnetopause over many spacecraft orbits, this is a reasonable
 141 assumption to make.

142 In these investigations and the present study, the location of the magnetopause bound-
 143 ary was found using in-situ data from the fluxgate magnetometer onboard the *Cassini*
 144 spacecraft, as documented by *Dougherty et al.* [2002]. *Arridge et al.* [2006] identified
 145 magnetopause crossings within the first six orbits of *Cassini*, between 28 June 2004 and
 146 28 March 2005. However, the high-latitude structure of the Kronian magnetosphere could
 147 not be investigated due to the limited coverage of these equatorial orbits.

148 In the absence of an upstream pressure monitor at Saturn, the solar wind dynamic pres-
 149 sure may be estimated by measuring the magnetic field inside the magnetopause and
 150 assuming that the total solar wind pressure, P_{SW} , balances the corresponding magnetic
 151 pressure,

$$P_{\text{SW}} = \frac{B^2}{2\mu_0} \cos^2 \Psi \quad (2)$$

152 where B is the magnetic field just inside the magnetopause, μ_0 is the magnetic permeabil-
 153 ity of free space and Ψ is the angle between the anti-solar wind direction and the normal
 154 to the magnetopause.

155 P_{SW} consists of two individual (but related) pressure contributions, the dynamic and static

156 pressures,

$$D_P + P_0 = \frac{B^2}{2\mu_0} \cos^2 \Psi \quad (3)$$

157 where P_0 is the static pressure and D_P denotes the dynamic pressure, the relative im-
 158 portance of these contributions depends on which part of the magnetopause is being
 159 considered. *Arridge et al.* [2006] set P_0 to a constant pressure of 10^{-4} nPa found from
 160 average solar wind values, using the work of *Slavin et al.* [1985]. However, the solar wind
 161 flows in curved streamlines around the magnetosphere which acts to reduce the pressure as
 162 opposed to the situation where the particles impact the boundary directly. *Petrinec and*
 163 *Russell* [1997] showed that applying Bernoulli's equation along the solar wind streamlines
 164 yields,

$$\frac{B^2}{2\mu_0} = kD_P \cos^2 \Psi + P_0 \sin^2 \Psi \quad (4)$$

165 k is the ratio of the pressure at the sub solar point to the upstream solar wind pressure
 166 [*Kanani et al.*, 2010] and is a factor that relates to how much the dynamic pressure is
 167 reduced when the plasma is considered to be flowing along streamlines. As the solar
 168 wind flows into the bow shock boundary and around the magnetopause, the streamlines
 169 diverge and the plasma is spread out as it flows around the obstacle and hence the flux
 170 of momentum across a given area is reduced. A value of 0.881 is appropriate in the case
 171 of a supersonic plasma.

172 The dynamic pressure dominates at small values of Ψ which corresponds to the nose of
 173 the magnetosphere. The static pressure dominates along the flanks of the magnetosphere
 174 where $\Psi \rightarrow 90^\circ$.

175 The formula of *Shue et al.* [1997] is used to model the magnetopause,

$$r = r_0(D_P, B_Z) \left(\frac{2}{1 + \cos \theta} \right)^{K(D_P, B_Z)} \quad (5)$$

176 where r is the distance from the centre of the planet to a point on the magnetopause
 177 surface, θ is the angle between the point and the planet-Sun line, r_0 is the magnetopause
 178 stand-off distance and K is an exponent that controls the flaring of the magnetopause.

179 This formalism is versatile as it can represent a variety of different magnetosphere mor-
 180 phologies. $K < 0.5$ represents a closed magnetosphere and $K > 0.5$ represents an open
 181 magnetosphere.

182 The original formalism developed by *Shue et al.* [1997] to model the terrestrial magneto-
 183 sphere included dependencies on the B_Z component of the IMF as well as the solar wind
 184 dynamic pressure. Since the IMF isn't thought to play a significant role in determining
 185 the size and shape of the magnetospheres of the outer planets, the relations were adapted
 186 by *Arridge et al.* [2006] into the form below,

$$r_0 = a_1 D_P^{-a_2} \quad (6)$$

$$K = a_3 + a_4 D_P \quad (7)$$

187
 188 the coefficients a_i were found by using a non-linear least squares fitting method to fit
 189 the the model magnetopause surface to the positions of the observed crossings. This
 190 procedure is performed iteratively, the coefficients found in the current iteration are used
 191 as a starting point in the next. The coefficients change with each successive iteration until
 192 they converge to within a tolerance of 10^{-6} .

193 The final estimates for the coefficients can in some cases depend on the initial estimates
 194 supplied to the solver. This issue is easily solved by repeating the fitting with different

195 starting values. *Arridge et al.* [2006] found the coefficients to be very stable and within
 196 their estimated uncertainties.

197 *Kanani et al.* [2010] improved on this model in several key ways. Firstly, the fixed static
 198 pressure was replaced by a more realistic form dependent on dynamic pressure. The ideal
 199 gas law is used to do this,

$$P_0 = nk_{\text{B}}T \quad (8)$$

200 where n and T are the number density and temperature of the solar wind and k_{B} is the
 201 Boltzmann constant. An expression for the dynamic pressure is then substituted,

$$D_{\text{P}} = \rho u_{\text{SW}}^2 \quad (9)$$

202 where u_{SW} is the upstream solar wind velocity.

203 The effects of plasma pressure are also included in the model of *Kanani et al.* [2010]. The
 204 *Cassini* electron plasma spectrometer (CAPS-ELS), as documented by *Young et al.* [2004],
 205 was used to find the pressure associated with electrons of energies between 0.8 eV and
 206 27 keV. Corresponding suprathermal ion pressures were found using data from *Cassini's*
 207 Magnetospheric Imaging Instrument (MIMI) as documented by *Krimigis et al.* [2004],
 208 which is capable of detecting ions with energies in the range 27-4000 keV.

209 Making these modifications, Equation 4 becomes,

$$kD_{\text{P}} \cos^2(\Psi) + \frac{k_{\text{B}}T_{\text{SW}}}{1.16m_p u_{\text{SW}}^2} D_{\text{P}} \sin^2(\Psi) = \frac{B^2}{2\mu_0} + P_{\text{MIMI}} + P_{\text{ELS}} \quad (10)$$

210 where P_{MIMI} is the pressure contribution of the suprathermal ions measured by the MIMI
 211 instrument and P_{ELS} is the pressure contribution of the electrons measured by the CAPS-
 212 ELS instrument. The factor of 1.16 has been introduced to account for the 4% abundance
 213 of He^{2+} in the solar wind which has a temperature approximately four times greater than

214 the protons, as found by *Slavin et al.* [1985].

215 *Kanani et al.* [2010] explored the sensitivity of the model to the value of this factor, as well
216 as the solar wind speed and the solar wind temperature but found that it was insensitive
217 to varying these parameters within reasonable limits.

2.2. Present Study

218 In this study, the polar confinement of Saturn's magnetosphere is quantified using a set
219 of magnetopause crossings between early 2007 and late 2008 in order to produce a more
220 complete picture of the dayside magnetopause of Saturn, including, for the first time, its
221 high-latitude structure. We use the techniques employed by *Kanani et al.* [2010] in order
222 to estimate the solar wind dynamic pressure in the absence of a dedicated upstream solar
223 wind monitor.

224 Comparisons between the dynamic pressure calculated assuming pressure balance and
225 that found by fitting the model through the exact location of each magnetopause crossing
226 are used in order to down-select the data and ensure that the magnetopause is close to
227 equilibrium at the time the spacecraft crosses the magnetosphere.

228 Finally, the phase of the global magnetic oscillation at Saturn is determined for each of
229 the magnetopause crossings in order to provide a preliminary check to determine if the
230 apparent flattening observed is predominantly a result of the global magnetic oscillations
231 (see Section 4.7 and the references therein) known to occur throughout the magnetosphere
232 of Saturn.

233 In addition, we have considered the pressure contribution associated with the centrifugal
234 force at the magnetopause as follows. A unit cross-section of the magnetopause layer has

235 centripetal force,

$$F_{CP} = mV R\omega^2 \quad (11)$$

236 where m is the mass per unit volume, V , ω is the angular velocity of the layer and R is
 237 the planet-layer distance. Considering the unit volume of the layer to be the unit area
 238 multiplied by the width of the layer then, by definition,

$$F_{CP} = \Delta F_{CF} \quad (12)$$

239 where Δ is the width of the layer and F_{CF} is the centrifugal force of the layer. Assuming,
 240 generously, that the magnetopause layer has similar density and rotation rate to the
 241 plasma just inside the magnetopause, the net force acting on this layer per unit area must
 242 supply the centripetal force in order to keep the plasma within the layer rotating, hence,

$$\frac{B^2}{2\mu_0} + P_{MIMI} - P_{SW} = -F_{CF}\Delta \quad (13)$$

243 From *Achilleos et al.* [2010] Figure 10 (lower panel), the centrifugal force per unit volume
 244 just inside the magnetopause is,

$$F_{CF} \sim 3 \cdot 10^{-9} \left(\frac{B_0^2}{\mu_0 R_S} \right) \quad (14)$$

245 where B_0 is the equatorial surface magnetic field strength with a typical value of
 246 ~ 20000 nT and R_S is the equatorial radius of Saturn with a value of 60280 km.

247 Hence,

$$F_{CF}\Delta \leq 3 \cdot 10^{-9} \left(\frac{B_0^2}{\mu_0} \right) \left(\frac{\Delta}{R_S} \right) \quad (15)$$

248 as, in reality, the density and rotation rate of the layer will be intermediate between
 249 those either side of the magnetopause. Also from *Achilleos et al.* [2010] Figure 10 (middle
 250 panel),

$$\left(\frac{B^2}{2\mu_0} + P_{MIMI} \right) \sim 0.02 \left(\frac{B_0^2}{\mu_0} \right) \quad (16)$$

251 thus,

$$\frac{F_{\text{CF}}\Delta}{\left(\frac{B^2}{2\mu_0} + P_{\text{MIMI}}\right)} \leq \left(\frac{3 \cdot 10^{-9}}{0.02}\right) \left(\frac{\Delta}{R_S}\right) \leq 10^{-7} \left(\frac{\Delta}{R_S}\right) \quad (17)$$

252 Δ is of the order $1 R_S$ [Masters et al., 2011]. Thus,

$$\frac{F_{\text{CF}}\Delta}{\left(\frac{B^2}{2\mu_0} + P_{\text{MIMI}}\right)} \leq 10^{-7} \quad (18)$$

253 hence the centrifugal force is very small compared to the magnetic and suprathermal
 254 plasma pressure gradients, and can safely be neglected.

3. Magnetopause Crossing Observations

255 For this study, we examined magnetometer data from the beginning of 2007 up until
 256 the very end of 2008 during which *Cassini* executed its first family of high-inclination
 257 orbits. Positive magnetopause crossing identifications were made in both the MAG and
 258 the CAPS-ELS datasets for each crossing used in the analysis.

259 Generally speaking, upon a transition from the magnetosheath to the magnetosphere, an
 260 increase in the total field strength as well as a rotation in the field is observed in the MAG
 261 data. In addition, the magnetic field is usually much steadier inside the magnetosphere.
 262 However, this is not always the case and a positive identification of a magnetopause cross-
 263 ing is not always possible using MAG data alone. In this situation, plasma data can
 264 provide complimentary information.

265 A sudden drop in the density of the plasma is observed in the CAPS-ELS data, typically
 266 by an order of magnitude, when the spacecraft passes from the magnetosheath to the
 267 magnetosphere. Also, the modal energy of the plasma just inside the magnetosphere is
 268 typically an order of magnitude greater than in the magnetosheath. As such, it is often
 269 much easier to detect magnetopause crossings in the CAPS-ELS data than the MAG data.

270 A series of magnetopause crossings are shown in Figure 1 which highlight some of these
271 tendencies.

272 *Kanani et al.* [2010] also included electron pressures derived from the CAPS-ELS in-
273 strument in their model, but found that the partial pressures of these electrons were on
274 average 1-2 orders of magnitude smaller than those associated with the magnetic field
275 and the suprathermal ions. This result allows us to neglect the electron pressure for the
276 purposes of this study.

277 Through careful analysis of the field and plasma data, 626 magnetopause crossings were
278 identified. Crossings within one hour of each other were averaged together, as it is likely
279 that these were caused by boundary waves in the magnetopause surface. Temporal aver-
280 aging of magnetopause crossings has been carried out in various forms by e.g. *Slavin and*
281 *Holzer* [1981]; *Slavin et al.* [1983, 1985]; *Huddleston et al.* [1998]. *Arridge et al.* [2006]
282 decided instead to average the crossings spatially to account for the different spacecraft
283 velocities of *Cassini* and *Voyager*. *Masters et al.* [2012a] found that boundary waves have
284 a period of ~ 3 hours on the dusk side of the planet, as such we have verified that the
285 results of this study are insensitive to averaging together crossings within this length of
286 time.

287 It is important to note that not all of the crossings have reliable suprathermal plasma
288 pressure moments. The hot plasma pressure moments, determined using MIMI, generally
289 have a resolution of 10 minutes, the minimum window usually required in order to have
290 reliable statistics for the computation of the moment. They are very variable in nature
291 and an increase by an order of magnitude from one 10 minute-average to the next is not
292 uncommon. The population contributing this pressure consists mainly of protons and ions

293 of oxygen (dominated by O^+). As oxygen ions are much more massive than protons, they
294 contribute about four times more to the total pressure than a proton of similar velocity.
295 As a result, it only takes a short interaction with a stream of these ions to increase the
296 total pressure by an order of magnitude (N. Sergis, private communication).

297 Further statistical measures have been used in order to reduce the effect of this on our
298 results. For each magnetopause crossing, the average magnetic field is taken inside the
299 magnetosphere as close to the crossing as possible, over a representative interval of time.
300 This interval must be long enough such that at least three measurements of the hot plasma
301 pressure moments are within it. The relative difference between the median and the up-
302 per and lower quartiles of the hot plasma pressure moment is then found; this difference
303 must be within a tolerance of 0.60 for the crossing to be accepted. The total number of
304 crossings for which there were reliable pressure moments available was 196.

305 The crossing locations are shown in Figure 2. The Kronocentric Solar Magnetospheric
306 (KSM) co-ordinate system has been used, in which the X -axis is directed from the planet
307 to the Sun and the Z -axis is such that the magnetic dipole axis of the planet lies within
308 the X - Z plane. The Y -axis completes the right-handed set and is thus pointed towards
309 dusk local time.

310 Much scatter can be seen in the crossing positions. This is because the observations have
311 been made over ~ 650 days and the magnetopause has thus experienced large variations
312 in shape and size, largely in response to variations in the solar wind dynamic pressure.

4. Magnetopause Modeling

4.1. Initial Results

313 For present purposes, it is firstly necessary to normalise the crossing locations to predict
 314 where the magnetopause boundary would be located at a fixed value of solar wind dynamic
 315 pressure. More specifically,

$$(X, Y, Z) = (X, Y, Z)_{\text{OBS}} \left(\frac{D_P}{\langle D_P \rangle} \right)^{\frac{1}{\alpha}} \quad (19)$$

316 where (X, Y, Z) and $(X, Y, Z)_{\text{OBS}}$ are the scaled and observed coordinates of the crossing
 317 location and $\langle D_P \rangle$ is a fixed pressure; the average dynamic pressure over all crossings was
 318 used in this case. Similar equations can be constructed for the other coordinates, as well
 319 as the radial distance from the planet centre. Although we normalise the crossings by
 320 D_P alone in this study, in reality the magnetic oscillation also affects the position of the
 321 magnetopause boundary. Here we assume that D_P is the dominant effect and neglect the
 322 effect of the magnetic oscillation, later in Section 4.7 we will present evidence to support
 323 this assumption.

324 The normalised crossings are shown in Figure 3 (a) along with representative X-Y slices
 325 of the axisymmetric model derived by *Kanani et al.* [2010] to form a contour map of the
 326 magnetosphere looking down onto the northern hemisphere. Although there is a degree
 327 of scatter (which will be discussed later in Section 4.2), the crossings at $Z_{\text{KSM}} \lesssim 10 R_S$
 328 tend to fit the slices well within an uncertainty of $1 - 2 R_S$.

329 However, as we increase Z_{KSM} (going from cooler colours to warmer colours in Figure 3 (a))
 330 the crossings seem to be systematically shifted away from the slices. This is particularly
 331 apparent for the crossings coloured from cyan-yellow on the colour scale, corresponding
 332 to $12-25 R_S$ Z_{KSM} .

333 A simple dilation of the magnetopause boundary along the Z_{KSM} direction has been used to
 334 construct a flattened magnetopause whereby Z_{KSM} in the axisymmetric boundary model

335 is replaced by $\mathcal{E}Z_{\text{KSM}}$. The factor \mathcal{E} governs the degree of flattening; a value smaller
 336 (greater) than 1 represents a flattened (inflated) magnetosphere.

337 In Figure 3 (b) a flattening of 20% (i.e. \mathcal{E} is equal to 0.80) has been applied to the model
 338 magnetopause surface. The positions of the crossings have changed somewhat, since the
 339 angle Ψ is found by fitting the magnetopause surface through each crossing as done by
 340 *Arridge et al.* [2006] (see Appendix A3 of that paper). Since the surface is now flattened,
 341 the angular separation between the normal to the surface and the X_{KSM} axis is now larger
 342 and therefore Ψ will be larger. This will result in a different estimate for D_P for each
 343 crossing following from Equation 10. This effect will be more pronounced for crossings
 344 at larger values of Z_{KSM} where the geometry of the magnetopause varies by the largest
 345 amount when this modification is applied.

346 In addition to this effect, some crossings present in the unflattened case may no longer
 347 be present when the magnetopause geometry is modified. This is because the Newton-
 348 Raphson iteration method used to fit the surface to each individual crossing cannot, in
 349 some cases, converge. The further the magnetopause is perturbed from the axisymmetric
 350 case by varying \mathcal{E} , the more difficult convergence seems to become.

351 There are no significant changes in the positions of the crossings between Figure 3. How-
 352 ever, the crossings and their corresponding X-Y slices are much closer together now for
 353 the crossings at large Z_{KSM} . This indicates that a surface flattened in the north-south
 354 direction is a better description for the magnetopause of Saturn, at least over the period
 355 at which these crossings were observed.

356 However, it is important to note that it is difficult to determine if the observed confinement
 357 is polar flattening, arising due to the disk-like nature of the obstacle to the solar wind flow,

358 or if it was caused by seasonal effects related to the hinging of the magnetosphere. Saturn
359 was approaching vernal (spring) equinox at the time that these observations were made,
360 its magnetic dipole was tilted away from the Sun by an angle ranging from $\sim 13^\circ - 4^\circ$. As
361 a result, seasonal effects may play some role in confining the magnetosphere, particularly
362 for the crossings near the start of the observation period.

363 The crossings at the largest values of Z_{KSM} (coloured orange and red in Figure 3) are of
364 great interest to this study. These unusual crossings are very far from the X - Y slices of
365 the same colour and clearly do not fit either model.

366 The plasma beta measured by the spacecraft for these crossings ranged between 15 and
367 25 and was exceptional compared to previous studies by *Sergis et al.* [2007, 2009] and
368 *Masters et al.* [2012b], who found that the plasma beta just inside the magnetopause can
369 be of the order 10.

370 It is possible that some form of transient event occurred during this time and was respon-
371 sible for energising the plasma or contributing more suprathermal plasma to the system
372 for this set of unusual crossings. In order to determine if a solar event may have caused
373 this energisation, the solar wind dynamic pressure estimated using the procedure outlined
374 above was compared to estimates from the Michigan Solar Wind Model (mSWiM) of
375 *Zieger and Hansen* [2008]. This model uses data taken from many near-Earth spacecraft
376 as an input and uses a one-dimensional MHD model to propagate this throughout the
377 solar system as far as 10 Au.

378 Its predictions are most accurate at near-apparent opposition between the Earth and the
379 object of interest and is reasonably accurate within 75 days of apparent opposition. For
380 Saturn, apparent opposition was at day 70 (11 March) 2007 which coincides with the

381 beginning of the data set we have chosen to analyse.

382 The crossings of interest are hence within the time period where the model is accurate.

383 However, the D_P predicted from our observations is approximately 60 times larger on
384 average than that predicted by mSWiM which implies that these high plasma betas were
385 not caused by a solar event.

386 The elevated plasma pressures observed for these crossings may be the result of ion conics
387 as described by *Mitchell et al.* [2009]; these can remain relatively steady over a period of
388 an hour or more. Alternatively, the magnetopause boundary may have simply been far
389 from equilibrium at the time that the spacecraft crossed it.

390 As these observations were made over a period of 4 days on different trajectories but in
391 similar regions of space, it is suggested that they could be related to a cusp region similar
392 to that suggested by the modelling work of *Maurice et al.* [1996]. *McAndrews et al.* [2008]
393 observed magnetic field and plasma signatures suggestive of reconnection events at Saturn
394 and found evidence of plasma energisation as a result. Since the cusp region is associated
395 with newly reconnected field lines, this energisation could be the explanation for the large
396 plasma beta values associated with these unusual crossings.

4.2. Monitoring Pressure Equilibrium at the Magnetopause

397 In accordance with the statistical law of large numbers, if a large number of measure-
398 ments of its position are made over a sufficient period of time, the magnetopause is likely
399 to be captured and depicted in an average state that is close to equilibrium.

400 Multi-spacecraft observations of the Earth's magnetopause by *Dunlop et al.* [2001] using
401 the four *Cluster* spacecraft found that strong and sudden accelerations of the magne-
402 topause boundary can occur. As such, some scatter may exist in our data where static

403 equilibrium of the boundary is not a good approximation.

404 Although we assumed that the magnetopause is in equilibrium at the outset of this study,
 405 we were able to quantify the departure from equilibrium as follows. A ‘global’ pressure es-
 406 timate was made for each magnetopause crossing by fitting the *Kanani et al.* [2010] model
 407 through each crossing and calculating the resulting pressure from the stand-off distance,
 408 r_0 , using Equation 6. The ratio between D_P and this new pressure estimate, referred to
 409 as P_{GLOB} , can then be calculated.

410 For an axisymmetric surface, the ratio $\frac{D_P}{P_{\text{GLOB}}}$ is expected to be unity at all points on the
 411 surface. When the surface departs from axisymmetry, the stand-off distance for an axisym-
 412 metric model fitted through any point on the surface where $Z_{\text{KSM}} \neq 0$ will be consistently
 413 underestimated compared to a flattened model, and hence P_{GLOB} will be consistently
 414 overestimated and the ratio will drop below unity.

415 This ratio was computed for each crossing and a histogram of the results plotted in Fig-
 416 ure 4. On top of this, the range indicated by the arrowed line shows the range of values
 417 expected based on using an axisymmetric model to estimate P_{GLOB} for a surface which is
 418 actually flattened ($\mathcal{E} = 0.80$).

419 The crossings follow a log-normal distribution which is largely enclosed by this interval but
 420 there exists some crossings that depart greatly from the expected range. These cannot be
 421 explained by the departure of the surface from axisymmetry and we suggest that they arise
 422 due to the departure of the surface from equilibrium, which is the underlying assumption
 423 made throughout this process. Hence, ratios that depart greatly from this range imply
 424 that the magnetopause was subject to strong accelerations at the time the observation
 425 was made. Values of $\frac{D_P}{P_{\text{GLOB}}}$ far from unity indicate a strong discrepancy between where

426 *Cassini* encountered the magnetopause and where it would have encountered it, had it
 427 been in equilibrium. As a result, this ratio can be used as a diagnostic to determine if the
 428 magnetopause was likely to be close to equilibrium when the spacecraft encountered it.
 429 In Figure 5 a new criterion has been included to filter the data set by removing any cross-
 430 ings where this ratio exceeds one interquartile range of the median (corresponding to an
 431 acceptance level of $\sim 2.4\sigma$). This reduces the number of magnetopause crossings to 158,
 432 down from 196. It can be seen by comparing Figure 3 to Figure 5 that the amount of
 433 scatter in the normalised positions of the crossings has been reduced considerably through
 434 the application of this criterion.

4.3. Statistical Tests

435 Let us consider the Wilcoxon signed rank test [Wilcoxon, 1945], applied to a subsample
 436 of our magnetopause crossings which lie in a given range $\{Z_0, Z_f\}$ of the Z_{KSM} coordinate.
 437 We will refer to this range as the ‘ Z_{KSM} band’ of this subsample.
 438 The quantity, $\Delta\rho$ to which we apply the rank sum test are defined as follows:

$$\Delta\rho_i = [(X_{\text{MP}}(Z_i, \mathcal{E}) - X_i)^2 + (Y_{\text{MP}}(Z_i, \mathcal{E}) - Y_i)^2]^{\frac{1}{2}} \quad (20)$$

439 the symbols here have the following meanings. There are N normalised crossings in the
 440 given Z_{KSM} band, and the i th crossing position is at (X_i, Y_i, Z_i) in KSM coordinates. The
 441 magnetopause surface is then constructed at $\langle D_P \rangle$, the pressure to which the crossings
 442 have been normalised, and the point on the slice through the X-Y plane at Z_i , closest to
 443 the normalised crossing location, has coordinates $(X_{\text{MP}}, Y_{\text{MP}}, Z_i)$. Hence $\Delta\rho_i$ represents a
 444 distance between each normalised crossing and the X-Y slice (at the same value of Z_{KSM})
 445 of a magnetopause model with a particular flattening parameter and is illustrated in Fig-

446 ure 6. The two sets of such distances we wish to compare are simply the $\Delta\rho_i$ evaluated
 447 for $\mathcal{E} = 1$ (the axisymmetric case) and $\mathcal{E} < 1$ (a flattened magnetopause model).

448 Let us represent these two sets of distances as $\Delta\rho_i(\mathcal{E} = 1)$ and $\Delta\rho_i(\mathcal{E} = 0.80)$ with
 449 $i = 1 \dots N$. As we shall see in the following analysis, $\mathcal{E} = 0.80$ appears to give values
 450 of $\Delta\rho_i$ significantly closer to 0 (i.e. a better agreement between modelled and observed
 451 magnetopause location) at high latitudes.

452 To apply the signed rank test, we order the union of both sets $\Delta\rho_i(\mathcal{E} = 1)$ and
 453 $\Delta\rho_i(\mathcal{E} = 0.80)$ in ascending order ignoring the signs, assigning a rank of 1 to the lowest
 454 absolute value, 2 to the second lowest absolute value, and so on. Each rank is then labelled
 455 with its sign according to the sign of $\Delta\rho_i$, s_i . If we denote these rank values as $rank(\Delta\rho_i)$,

456 then the rank sums of the two distance sets are defined as $|\sum_{i=1}^n s_i \cdot rank(\Delta\rho_i(\mathcal{E} = 1))|$ and

$$457 \left| \sum_{i=1}^n s_i \cdot rank(\Delta\rho_i(\mathcal{E} = 0.80)) \right|.$$

458 The test statistic, W , is the rank sum of either group of $\Delta\rho_i$ values. The test itself con-
 459 sists of comparing W with a critical value $S(p, N)$. This value $S(p, N)$ denotes that, if
 460 the the null hypothesis is true (i.e. the median values of the underlying $\Delta\rho_i$ distributions
 461 are zero), there is a probability p that W would exceed $S(p, N)$. Table 1 indicates the
 462 value of p for which $W = S(p, N)$ for different Z_{KSM} bands. This tabulated value may be
 463 thought of as the probability that the magnetopause crossings would have a signed rank
 464 equal to or exceeding their observed value, given that they correspond to a magnetopause
 465 with a given flattening parameter \mathcal{E} .

466 The results of this test applied to the data shown in Figure 7 are shown in Table 1. In
 467 each case, the p -value when a flattening is applied to the model magnetopause is larger
 468 than that of the axisymmetric model, which indicates that, on average, flattening the

469 magnetopause surface causes it to move closer to the crossing positions and hence a flat-
 470 tened surface is a better fit to the data.

471 This test is powerful as it doesn't rely on the population being normally distributed unlike
 472 similar tests, for example the Student's t-test. However, it does assume that the popula-
 473 tion is symmetric. The adjusted Fisher-Pearson standardised moment coefficient [*Doane*
 474 *and Seward, 2011*] provides a measure of sample symmetry and has been calculated for
 475 each Z_{KSM} band to determine if it is, indeed, symmetric and, hence, if the Wilcoxon signed
 476 rank test applies. A coefficient of zero indicates that the data is perfectly symmetric, how-
 477 ever this is very unlikely for real-world data. *Doane and Seward [2010]* compiled a table of
 478 sample skewness coefficients corrected for sample size. We compare the results of this test
 479 of symmetry against these criteria to determine that each band of Z_{KSM} is approximately
 480 symmetric as the calculated coefficients are well within their limits. As such, we deem
 481 the Wilcoxon signed rank test to be appropriate for our data.

4.4. Uncertainty in \mathcal{E}

482 It became clear that the value of \mathcal{E} that provided the best fit between the model and
 483 the data is dependant on the distribution of the magnetopause crossings within the bands
 484 of Z_{KSM} . Hence it is also dependant on the binning process itself. We have used this fact
 485 to estimate the uncertainty in our estimate of \mathcal{E} .

486 For each estimate of \mathcal{E} , the bands have been spaced evenly by $Z_{\text{KSM}} = \Delta Z_{\text{KSM}}$. To ensure
 487 that a significant number of crossings lie within each band, the minimum value chosen for
 488 ΔZ_{KSM} was $5 R_S$ and this was increased in steps of $1 R_S$ up to a maximum value of $10 R_S$.
 489 As there are many more crossings at smaller values of Z_{KSM} , it was found that bands at
 490 values of Z_{KSM} between $20\text{-}35 R_S$ were sparsely populated. Crossings in these bands were

491 moved down to the band below until a minimum of 25 crossings occupied each band since
492 it is difficult to determine if a sample smaller than 25 is symmetric. This ensures that
493 there are statistically enough crossings within each band to enable us to draw conclusions
494 from the data.

495 This procedure yielded a mean, modal and median value of \mathcal{E} of 0.82 with an uncertainty
496 of ± 0.03 indicating a polar confinement of $20\% \pm 3\%$.

497 A second uncertainty estimate has been made using a Monte Carlo (BCa bootstrap)
498 method. Here, the same procedure used to determine \mathcal{E} in Section 4.3 is used, but this time
499 N crossings are randomly drawn with replacement from our population of N crossings.
500 As the crossings are drawn with replacement, a different set of crossings are drawn for
501 each resampling and, as a result, the best fitting value of \mathcal{E} changes. This was repeated
502 2000 times and \mathcal{E} was found to be 0.81 within a confidence interval of 0.75-0.84 at the
503 68.3% (1σ) confidence level.

4.5. Magnetopause Pressure Dependence

504 The reduced set of crossings has been separated into two groups in Figure 8, one where
505 the estimated dynamic pressure is above the average and where it is below. There seems
506 to be a better distribution of crossings with low D_P whereas the crossings at high D_P
507 seem to be clustered within 3 regions of local time.

508 The same techniques as previously discussed have been used to determine the value of
509 \mathcal{E} that provides the best fit between the model and each data sample. For the low D_P
510 crossings, a value of \mathcal{E} of 0.75 within a confidence interval of 0.71 - 0.82 provides the
511 best fit whereas for the high D_P crossings a value of 0.79 within a confidence interval of
512 0.78 - 0.93 was found. Hence, within the given uncertainties and for the range of dynamic

513 pressures considered here, the polar confinement of the magnetosphere is insensitive to
 514 changes in dynamic pressure.

515 The flaring parameter, K , is the same in both cases within its uncertainty, based on the
 516 uncertainties in the model parameters determined by *Kanani et al.* [2010]. This contrasts
 517 with the study by *Huddleston et al.* [1998] who found the Jovian magnetosphere to be
 518 more streamlined at high D_P .

4.6. Trajectory Analysis

519 In order to be sure that we are adequately sampling the mean position of the boundary,
 520 we need to analyse the spacecraft trajectory and ensure that, even for the high-latitude
 521 passes, there is a clear transition between where we spend 50% of the time inside, and
 522 50% outside, the magnetosphere. A similar method to that employed by *Joy et al.* [2002]
 523 in the case of Jupiter and subsequently employed by *Achilleos et al.* [2008] in the case of
 524 Saturn is used here. The procedure is as follows:

525 1. Magnetopause crossings are located and the spacecraft trajectory is split into small
 526 time intervals. It is important that the list of crossings is as complete as possible to obtain
 527 accurate results. It is also important that the sampling time scale is small compared to
 528 the time between crossings. An interval of 10 minutes is used here.

529 2. At each point along the magnetopause trajectory, the magnetopause crossings are
 530 used to determine if the spacecraft is inside or outside of the magnetosphere and

531 $\rho_{\text{KSM}} = \sqrt{Y_{\text{KSM}}^2 + Z_{\text{KSM}}^2}$ and $\phi_{\text{KSM}} = \tan^{-1} \left(\frac{Z_{\text{KSM}}}{Y_{\text{KSM}}} \right)$ are calculated at each point in time.

532 Occasionally this may be impossible due to a data gap or other such anomaly, in which
 533 case this interval is discarded.

534 3. Separate the crossings into bins of X_{KSM} of width ΔX_{KSM} such that there are N_X

bins with centres X_{KSM}^i for $i = 1 \dots N_X$. Further subdivide bins X_{KSM}^i into bins of ρ_{KSM} of
width $\Delta\rho_{\text{KSM}}$ with centres ρ_{KSM}^j for $j = 1 \dots N_\rho$ such that there are now $N_X N_\rho$ bins each
containing $M_{I_{ij}}$ data points inside the magnetosphere and $M_{O_{ij}}$ data points outside the
magnetosphere.

4. For each X_{KSM}^i bin, calculate the probability distribution of ρ_{KSM} . The prob-
ability that the actual value of ρ_{KSM} exceeds that of ρ_{KSM}^j can be estimated as

$$P(\rho_{\text{KSM}} > \rho_{\text{KSM}}^j) = M_{I_{ij}} / (M_{I_{ij}} + M_{O_{ij}}).$$

5. For each X_{KSM}^i bin, identify if there is a clear ‘transition distance’, ρ_{KSM}^T , where the
spacecraft spends 50% of the time inside, and 50% outside, the magnetosphere. If this is
the case, the magnetopause is being adequately sampled by the trajectories along which
the magnetopause crossings are identified for that particular bin of X_{KSM} .

The data points were then separated into two groups based on their ϕ_{KSM} angles into
equatorial ($\phi_{\text{KSM}} < 50^\circ$) and high-latitude ($\phi_{\text{KSM}} > 50^\circ$) parts of the trajectory. These
data limits are valid only for magnetopause crossings in the northern hemisphere/near-
equatorial southern magnetopause crossings.

Figure 9 shows the results of following this procedure for our dataset. Included are error
bars determined using a Monte Carlo Bootstrap method ran 1000 times for each X_{KSM}^i bin
at the 3σ (99.7%) level. It shows that in most cases, the transition distance is captured
and hence the magnetopause is being adequately sampled. Figure 9 (b) shows the results
for the high-latitude parts of the trajectory. Most of the high-latitude crossings that show
a large degree of flattening were in the $X_{\text{KSM}} = 0 - 25 R_S$ range as can be seen in Figure
2 (b). We capture the transition distance in all but one of the X_{KSM}^i bins in this range.

557 In addition to this, on average the transition distance is a few R_S smaller in the polar
 558 dataset than in the equatorial dataset, consistent with a polar confinement.

4.7. Phase of the Global Magnetic Oscillation

559 As mentioned previously, the planetary-period magnetic oscillation that has been ob-
 560 served at Saturn is likely to have had an effect on the position of the magnetopause
 561 crossings used in this study. For the current study, this oscillation is not taken into ac-
 562 count and is treated as noise.

563 However, a small investigation has been undertaken to determine if the apparent flattening
 564 of the magnetosphere is caused by this magnetic oscillation. To do this, the SLS3 longitu-
 565 dinal system of *Kurth et al.* [2008] has been used. The SLS3 longitude of the spacecraft at
 566 each crossing has been calculated and plotted in Figure 10 (a). The longitude of the peak
 567 phase front (defined as 100° longitude in the SLS3 system) has also been plotted taking
 568 into account bend back effects due to the finite wave speed using parameters determined
 569 by *Arridge et al.* [2011]. Specifically, the distance at which the plasma sheet becomes
 570 tilted is taken as $12 R_S$ and the phase delay is taken as $6.7^\circ R_S^{-1}$. The difference in phase
 571 between the crossings and the peak phase front have been plotted in Figure 10 (b) against
 572 the Z_{KSM} coordinate of the crossing.

573 The key result displayed in Figure 10 is that there is no evidence of a pattern between the
 574 distribution of the crossings in the SLS3 system and the Z_{KSM} coordinate. The relevant
 575 crossings at large Z_{KSM} are distributed fairly evenly in SLS3 longitude. If the magne-
 576 topause flattening was highly dependant on the magnetic oscillation then it would be
 577 expected that the crossings at larger Z_{KSM} would be clustered together at a similar lon-
 578 gitude in the SLS3 system, but this is not the case.

579 In addition to this, if the magnetic oscillation was the dominant influence on the high-
580 latitude boundary location, the normalised boundary locations at large Z_{KSM} would be
581 scattered evenly around the axisymmetric model boundary. This is not the case as most
582 of these crossings lie inside the axisymmetric surface as can be seen in Figures 3 and 5.

5. Discussion

583 We have investigated the structure of the magnetopause of Saturn using in-situ *Cassini*
584 data paying particular attention to the high-latitude regions which haven't previously
585 been studied in detail. Magnetometer and electron plasma spectrometer data has been
586 used to identify magnetopause crossings from a set of highly inclined orbits and estimate
587 the solar wind dynamic pressure at each crossing.

588 This allowed us to normalise the crossings to a fixed pressure so that we could fit models
589 to the data to determine if the magnetosphere of Saturn exhibits polar flattening as has
590 been observed at Jupiter by *Huddleston et al.* [1998]. Even so, a considerable amount
591 of scatter is present in the data and further measures were taken to reduce this by com-
592 paring two different pressure estimates for each crossing and removing those where these
593 estimates deviate by more than a factor of 3.

594 By applying a simple dilation to the axisymmetric magnetopause boundary in the Z_{KSM}
595 direction, a north-south flattening of 19% within a confidence interval of 13-22% has been
596 found compared to the axisymmetric case.

597 The magnetopause crossings identified in this investigation are limited almost exclusively
598 to the dusk sector of the magnetopause and all of those in dawn sector are located at
599 equatorial latitudes. Future studies should include crossings from the dawn sector such
600 that east-west asymmetries in the structure of the magnetopause can be identified.

601 Seasonal variations are expected due to the hinging effect of the magnetodisc and the
602 north-south asymmetry that this introduces to the magnetic field structure of the mag-
603 netosphere. The magnetopause crossings used in this study were located when the planet
604 was approaching the vernal equinox with a dipole tilt angle of $\sim 13^\circ - 4^\circ$. A similar study
605 performed at a different planetary season may reveal what effects the hinging of the mag-
606 netodisc has on the structure of the magnetopause.

607 Additional layers of complexity could be added to the model in future studies to improve
608 its fit to the data. The phase of the magnetic oscillation has been briefly touched upon in
609 this study to determine if it could explain the apparent polar flattening that we observe.
610 It was found that the crossings at high Z_{KSM} where we see a large degree of polar flat-
611 tening are not at a similar oscillation phase which indicates it is not the cause. However,
612 the oscillation should have some degree of an effect on the location of the magnetopause
613 as found by *Clarke et al.* [2006], and it is likely that if this effect was properly taken into
614 account in future studies, there would be less scatter in the positions of the normalised
615 crossings.

616
617 **Acknowledgments.** N.M.P thanks the UK Science and Technology Facilities Council
618 (STFC) for their support (grant code ST/K502406/1) through a PhD studentship.

References

619 Achilleos, N., C. S. Arridge, C. Bertucci, C. M. Jackman, M. K. Dougherty, K. K.
620 Khurana, and C. T. Russell (2008), Large-scale dynamics of Saturn's magnetopause:
621 Observations by Cassini, *Journal of Geophysical Research*, *113*(A11), 1–14, doi:

622 10.1029/2008JA013265.

623 Achilleos, N., P. Guio, and C. S. Arridge (2010), A model of force balance in Saturn's
624 magnetodisc, *Monthly Notices of the Royal Astronomical Society*, *401*(4), 2349–2371,
625 doi:10.1111/j.1365-2966.2009.15865.x.

626 Andrews, D. J., E. J. Bunce, S. W. H. Cowley, M. K. Dougherty, G. Provan, and D. J.
627 Southwood (2008), Planetary period oscillations in Saturn's magnetosphere: Phase rela-
628 tion of equatorial magnetic field oscillations and Saturn kilometric radiation modulation,
629 *Journal of Geophysical Research*, *113*(A9), A09,205, doi:10.1029/2007JA012937.

630 Andrews, D. J., S. W. H. Cowley, M. K. Dougherty, L. Lamy, G. Provan, and D. J.
631 Southwood (2012), Planetary period oscillations in Saturn's magnetosphere: Evolution
632 of magnetic oscillation properties from southern summer to post-equinox, *Journal of*
633 *Geophysical Research*, *117*(A4), A04,224, doi:10.1029/2011JA017444.

634 Arridge, C. S., N. Achilleos, M. K. Dougherty, K. K. Khurana, and C. T. Russell (2006),
635 Modeling the size and shape of Saturn's magnetopause with variable dynamic pressure,
636 *Journal of Geophysical Research*, *111*(A11), 1–13, doi:10.1029/2005JA011574.

637 Arridge, C. S., N. André, K. K. Khurana, C. T. Russell, S. W. H. Cowley, G. Provan,
638 D. J. Andrews, C. M. Jackman, A. J. Coates, E. C. Sittler, M. K. Dougherty, and
639 D. T. Young (2011), Periodic motion of Saturn's nightside plasma sheet, *Journal of*
640 *Geophysical Research*, *116*(A11), A11,205, doi:10.1029/2011JA016827.

641 Bagenal, F. (1992), Giant Planet Magnetospheres, *Annual Review of Earth and Planetary*
642 *Science*, *20*, 289–328.

643 Clarke, K. E., N. André, D. J. Andrews, A. J. Coates, S. W. H. Cowley, M. K. Dougherty,
644 G. R. Lewis, H. J. McAndrews, J. D. Nichols, T. R. Robinson, and D. M. Wright

- 645 (2006), Cassini observations of planetary-period oscillations of Saturn's magnetopause,
646 *Geophysical Research Letters*, *33*(23), L23,104, doi:10.1029/2006GL027821.
- 647 Clarke, K. E., D. J. Andrews, C. S. Arridge, A. J. Coates, and S. W. H. Cow-
648 ley (2010), Magnetopause oscillations near the planetary period at Saturn: Occur-
649 rence, phase, and amplitude, *Journal of Geophysical Research*, *115*(A8), A08,209, doi:
650 10.1029/2009JA014745.
- 651 Cowley, S. W. H., D. M. Wright, E. J. Bunce, a. C. Carter, M. K. Dougherty, G. Giampieri,
652 J. D. Nichols, and T. R. Robinson (2006), Cassini observations of planetary-period
653 magnetic field oscillations in Saturn's magnetosphere: Doppler shifts and phase motion,
654 *Geophysical Research Letters*, *33*(7), L07,104, doi:10.1029/2005GL025522.
- 655 Dessler, A. J. (1980), Mass-injection rate from Io into the Io plasma torus, *Icarus*, *44*(2),
656 291–295, doi:10.1016/0019-1035(80)90024-X.
- 657 Doane, D., and L. Seward (2010), *Applied Statistics in Business and Economics*, 864 pp.,
658 McGraw-Hill Higher Education.
- 659 Doane, D. P., and L. E. Seward (2011), Measuring Skewness : A Forgotten Statistic ?,
660 *Journal of Statistic Education*, *19*(2), 1–18.
- 661 Dougherty, M. K., S. Kellock, D. J. Southwood, A. Balogh, E. J. Smith, B. T. Tsurutani,
662 B. Gerlach, F. Gleim, C. T. Russell, G. Erdos, F. M. Neubauer, and S. W. H. Cowley
663 (2002), The cassini magnetic field investigation, *Space Science Reviews*, pp. 331–383.
- 664 Dunlop, M. W., A. Balogh, P. Cargill, R. C. Elphic, K.-H. Fornacon, E. Georgescu,
665 and F. Sedgemore-Schulthess (2001), Cluster observes the Earths magnetopause: coor-
666 dinated four-point magnetic field measurements, *Annales Geophysicae*, *19*(February),
667 1449–1460.

- 668 Espinosa, S. A., and M. K. Dougherty (2000), Periodic perturbations in Saturn's magnetic
669 field, *Geophysical Research Letters*, *27*(17), 2785–2788.
- 670 Espinosa, S. A., and M. K. Dougherty (2001), Unexpected periodic perturbations in Sat-
671 urn's magnetic field data from Pioneer 11 and Voyager 2, *Advances in Space Research*,
672 *28*(6), 919–924, doi:10.1016/S0273-1177(01)00518-X.
- 673 Espinosa, S. A., D. J. Southwood, and M. K. Dougherty (2003), How can Saturn impose
674 its rotation period in a noncorotating magnetosphere?, *Journal of Geophysical Research*,
675 *108*(A2), 1086, doi:10.1029/2001JA005084.
- 676 Huddleston, D. E., C. T. Russell, M. G. Kivelson, K. K. Khurana, and L. Bennett (1998),
677 Location and shape of the Jovian magnetopause and bow shock, *Journal of Geophysical*
678 *Research*, *103*(E9), 75–82.
- 679 Jia, X., K. C. Hansen, T. I. Gombosi, M. G. Kivelson, G. Tóth, D. L. DeZeeuw, and A. J.
680 Ridley (2012), Magnetospheric configuration and dynamics of Saturn's magnetosphere:
681 A global MHD simulation, *Journal of Geophysical Research*, *117*(A5), A05,225, doi:
682 10.1029/2012JA017575.
- 683 Joy, S. P., M. G. Kivelson, R. J. Walker, K. K. Khurana, C. T. Russell, and T. Ogino
684 (2002), Probabilistic models of the Jovian magnetopause and bow shock locations, *Jour-*
685 *nal of Geophysical Research*, *107*(A10), 1–17, doi:10.1029/2001JA009146.
- 686 Kanani, S. J., C. S. Arridge, G. H. Jones, A. N. Fazakerley, H. J. McAndrews, N. Sergis,
687 S. M. Krimigis, M. K. Dougherty, A. J. Coates, D. T. Young, K. C. Hansen, and
688 N. Krupp (2010), A new form of Saturn's magnetopause using a dynamic pressure
689 balance model, based on in situ, multi-instrument Cassini measurements, *Journal of*
690 *Geophysical Research*, *115*(A6), 1–11, doi:10.1029/2009JA014262.

- 691 Kivelson, M. G., and D. J. Southwood (2005), Dynamical consequences of two modes
692 of centrifugal instability in Jupiter’s outer magnetosphere, *Journal of Geophysical Re-*
693 *search*, *110*(A12), A12,209, doi:10.1029/2005JA011176.
- 694 Krimigis, S. M., D. G. Mitchell, D. C. Hamilton, S. Livi, J. Dandouras, S. Jaskulek,
695 T. P. Armstrong, J. D. Boldt, A. F. Cheng, G. Gloeckler, J. R. Hayes, K. C. Hsieh,
696 E. P. Keath, E. Kirsch, N. Krupp, L. J. Lanzerotti, R. Lundgren, B. H. Mauk, R. W.
697 Mcentire, E. C. Roelof, C. E. Schlemm, B. E. Tossman, B. Wilken, and D. J. Williams
698 (2004), MAGNETOSPHERE IMAGING INSTRUMENT (MIMI) ON THE CASSINI
699 MISSION TO SATURN / TITAN, *Space Science Reviews*, *114*, 233–329.
- 700 Kurth, W. S., T. F. Averkamp, D. a. Gurnett, J. B. Groene, and a. Lecacheux (2008), An
701 update to a Saturnian longitude system based on kilometric radio emissions, *Journal of*
702 *Geophysical Research*, *113*(A5), A05,222, doi:10.1029/2007JA012861.
- 703 Masters, A., D. G. Mitchell, A. J. Coates, and M. K. Dougherty (2011), Saturn’s low-
704 latitude boundary layer: 1. Properties and variability, *Journal of Geophysical Research*,
705 *116*(A6), A06,210, doi:10.1029/2010JA016421.
- 706 Masters, A., N. Achilleos, J. Cutler, A. J. Coates, M. K. Dougherty, and G. H. Jones
707 (2012a), Surface waves on Saturn’s magnetopause, *Planetary and Space Science*, *65*(1),
708 109–121, doi:10.1016/j.pss.2012.02.007.
- 709 Masters, A., J. P. Eastwood, M. Swisdak, M. F. Thomsen, C. T. Russell, N. Sergis, F. J.
710 Crary, M. K. Dougherty, A. J. Coates, and S. M. Krimigis (2012b), The importance of
711 plasma β conditions for magnetic reconnection at Saturn’s magnetopause, *Geophysical*
712 *Research Letters*, *39*(8), L08,103, doi:10.1029/2012GL051372.

- 713 Maurice, S., I. M. Engle, M. Blanc, and M. Skubis (1996), Geometry of Saturn's magne-
714 topause model, *Journal of Geophysical Research*, *101*(A12), 27,053–9.
- 715 McAndrews, H. J., C. J. Owen, M. F. Thomsen, B. Lavraud, A. J. Coates,
716 M. K. Dougherty, and D. T. Young (2008), Evidence for reconnection at Sat-
717 urn's magnetopause, *Journal of Geophysical Research*, *113*(A4), A04,210, doi:
718 10.1029/2007JA012581.
- 719 Mitchell, D. G., W. S. Kurth, G. B. Hospodarsky, N. Krupp, J. Saur, B. H. Mauk, J. F.
720 Carbary, S. M. Krimigis, M. K. Dougherty, and D. C. Hamilton (2009), Ion conics and
721 electron beams associated with auroral processes on Saturn, *Journal of Geophysical*
722 *Research*, *114*(A2), A02,212, doi:10.1029/2008JA013621.
- 723 Parker, E. N. (1958), Dynamics of the Interplanetary Gas and Magnetic Fields, *American*
724 *Astronomical Society*, *128*, 664–75.
- 725 Petrinec, S. M., and C. T. Russell (1997), Hydrodynamic and MHD Equations Across the
726 Bow Shock and Along the Surfaces of Planetary Obstacles, *Space Science Reviews*, *79*,
727 757–791.
- 728 Pontius, D. H., and T. W. Hill (2006), Enceladus: A significant plasma source
729 for Saturn's magnetosphere, *Journal of Geophysical Research*, *111*(A9), 1–8, doi:
730 10.1029/2006JA011674.
- 731 Provan, G., D. J. Andrews, B. Cecconi, S. W. H. Cowley, M. K. Dougherty, L. Lamy, and
732 P. M. Zarka (2011), Magnetospheric period magnetic field oscillations at Saturn: Equa-
733 torial phase jitter produced by superposition of southern and northern period oscilla-
734 tions, *Journal of Geophysical Research*, *116*(A4), A04,225, doi:10.1029/2010JA016213.

- 735 Provan, G., D. J. Andrews, C. S. Arridge, A. J. Coates, S. W. H. Cowley, G. Cox, M. K.
736 Dougherty, and C. M. Jackman (2012), Dual periodicities in planetary-period magnetic
737 field oscillations in Saturn's tail, *Journal of Geophysical Research*, *117*(A1), A01,209,
738 doi:10.1029/2011JA017104.
- 739 Provan, G., S. W. H. Cowley, J. Sandhu, D. J. Andrews, and M. K. Dougherty (2013),
740 Planetary period magnetic field oscillations in Saturn's magnetosphere: Post-equinox
741 abrupt non-monotonic transitions to northern system dominance, *Journal of Geophys-*
742 *ical Research: Space Physics*, pp. n/a–n/a, doi:10.1002/jgra.50186.
- 743 Sergis, N., S. M. Krimigis, D. G. Mitchell, D. C. Hamilton, N. Krupp, B. M. Mauk, E. C.
744 Roelof, and M. K. Dougherty (2007), Ring current at Saturn: Energetic particle pres-
745 sure in Saturn's equatorial magnetosphere measured with Cassini/MIMI, *Geophysical*
746 *Research Letters*, *34*(9), L09,102, doi:10.1029/2006GL029223.
- 747 Sergis, N., S. M. Krimigis, D. G. Mitchell, D. C. Hamilton, N. Krupp, B. H. Mauk, E. C.
748 Roelof, and M. K. Dougherty (2009), Energetic particle pressure in Saturn's magneto-
749 sphere measured with the Magnetospheric Imaging Instrument on Cassini, *Journal of*
750 *Geophysical Research*, *114*(A2), A02,214, doi:10.1029/2008JA013774.
- 751 Shue, J. H., J. K. Chao, H. C. Fu, C. T. Russell, P. Song, K. K. Khurana, and H. J. Singer
752 (1997), A new functional form to study the solar wind control of the magnetopause size
753 and shape, *Journal of Geophysical Research-Space Physics*, *102*(A5), 9497–9511, doi:
754 10.1029/97JA00196.
- 755 Slavin, J. a., and R. E. Holzer (1981), Solar wind flow about the terrestrial planets 1.
756 Modeling bow shock position and shape, *Journal of Geophysical Research*, *86*(A13),
757 11,401, doi:10.1029/JA086iA13p11401.

- 758 Slavin, J. A., E. J. Smith, P. R. Gazis, and J. D. Mihalov (1983), A Pioneer-Voyager
759 Study of the Solar Wind Interaction with Saturn, *Geophysical Research Letters*, *10*(1),
760 9–12.
- 761 Slavin, J. a., E. J. Smith, J. R. Spreiter, and S. S. Stahara (1985), Solar wind flow about
762 the outer planets: Gas dynamic modeling of the Jupiter and Saturn bow shocks, *Journal*
763 *of Geophysical Research*, *90*(A7), 6275, doi:10.1029/JA090iA07p06275.
- 764 Slavin, J. a., S. M. Krimigis, M. H. Acuna, B. J. Anderson, D. N. Baker, P. L. Koehn,
765 H. Korth, S. Livi, B. H. Mauk, S. C. Solomon, and T. H. Zurbuchen (2007), MESSEN-
766 GER: Exploring Mercurys Magnetosphere, *Space Science Reviews*, *131*(1-4), 133–160,
767 doi:10.1007/s11214-007-9154-x.
- 768 Snyder, C. V., and M. Neugebauer (1963), The Solar Wind Velocity and Its Correlation
769 with Cosmic-Ray Variationad and with Solar and Geomagnetic Activity, *Journal of*
770 *Geophysical Research*, *68*(24), 6361–70.
- 771 Spencer, J. (2011), Watery Enceladus, *Physics Today*, *64*(11), 38, doi:10.1063/PT.3.1331.
- 772 Tokar, R. L., R. E. Johnson, T. W. Hill, D. H. Pontius, W. S. Kurth, F. J. Crary, D. T.
773 Young, M. F. Thomsen, D. B. Reisenfeld, A. J. Coates, G. R. Lewis, E. C. Sittler, and
774 D. A. Gurnett (2006), The Interaction of the Atmosphere of enceladus with Saturn’s
775 Plasma, *Science*, *311*, 1409–12, doi:10.1126/science.1121061.
- 776 Waite, J. H. J., W. S. Lewis, B. a. Magee, J. I. Lunine, W. B. McKinnon, C. R. Glein,
777 O. Mousis, D. T. Young, T. Brockwell, J. Westlake, M.-J. Nguyen, B. D. Teolis, H. B.
778 Niemann, R. L. McNutt, M. Perry, and W.-H. Ip (2009), Liquid water on Enceladus
779 from observations of ammonia and ^{40}Ar in the plume, *Nature*, *460*(7254), 487–490,
780 doi:10.1038/nature08153.

Table 1. Results of Statistical Tests

Wilcoxon Signed Rank Test	$Z_{\text{KSM}} < 5 R_{\text{S}}$	$5 < Z_{\text{KSM}} < 10 R_{\text{S}}$	$Z_{\text{KSM}} > 10 R_{\text{S}}$
Unflattened p -value	0.01 (70)	0.07 (48)	0.00 (40)
Flattened p -value	0.03 (70)	0.66 (47)	0.72 (41)

781 Wilcoxon, F. (1945), Individual Comparisons by Ranking Methods Frank Wilcoxon, *Bio-*
782 *metrics Bulletin*, 1(6), 80–83.

783 Young, D. T., J. J. Berthelier, M. Blanc, J. L. Burch, A. J. Coates, R. Goldstein,
784 M. Grande, T. W. Hill, R. E. Johnson, V. Kelha, D. J. McComas, E. C. Sittler, K. R.
785 Svenes, and K. Szego (2004), Cassini Plasma Spectrometer Investigation, *Space Science*
786 *Reviews*, 114, 1–112.

787 Zieger, B., and K. C. Hansen (2008), Statistical validation of a solar wind propagation
788 model from 1 to 10 AU, *Journal of Geophysical Research*, 113(A8), A08,107, doi:
789 10.1029/2008JA013046.

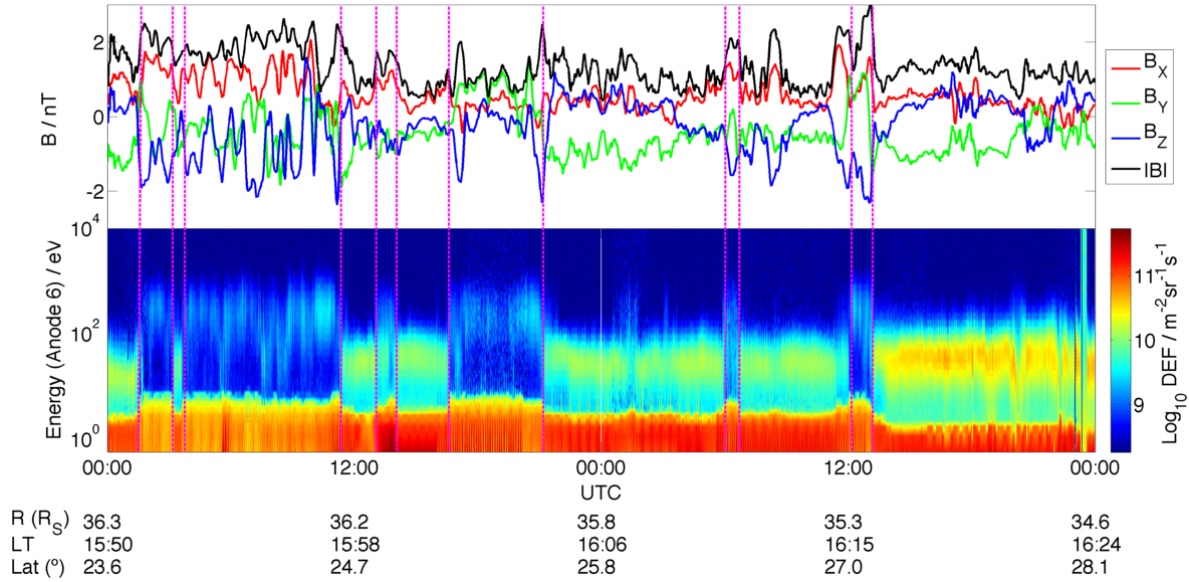


Figure 1. In-situ data taken by the *Cassini* spacecraft over 48 hours starting at midnight on day 123 of 2007 (3 May). The upper panel shows the components of the magnetic field as well as its magnitude with a one-minute time resolution smoothed using a moving average filter with a span of 11 minutes'. The lower panel shows an electron spectrogram from the CAPS-ELS instrument. The energy and count rate (which is proportional to density) of the electrons are represented logarithmically. The vertical magenta lines indicate magnetopause crossings, 12 such crossings can be seen during this period characterised by sudden changes in electron energy and count rate and magnetic field strength, as well as rotations in the magnetic field. The persistent population of low energy (< 10 eV) electrons are photoelectrons.

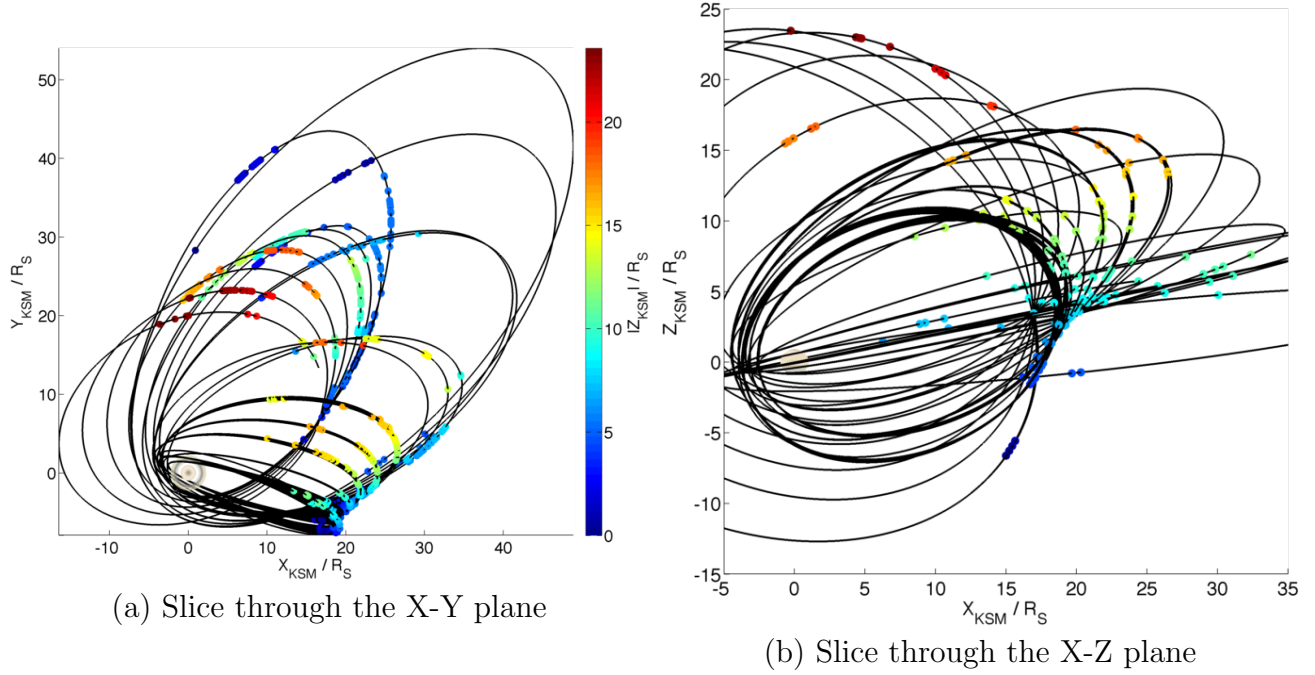


Figure 2. The lines show consecutive orbits of the *Cassini* spacecraft and the points are locations where a magnetopause crossing has been identified. Each crossing is coloured according to its Z_{KSM} coordinate. (a) is looking from the dawn side to the dusk side of the magnetosphere. It shows the high-latitude coverage of the spacecraft within the time period that this study covers. (b) is looking down on the magnetosphere from the pole of the northern hemisphere. It shows that the majority of the crossings are confined to the noon-dusk sector.

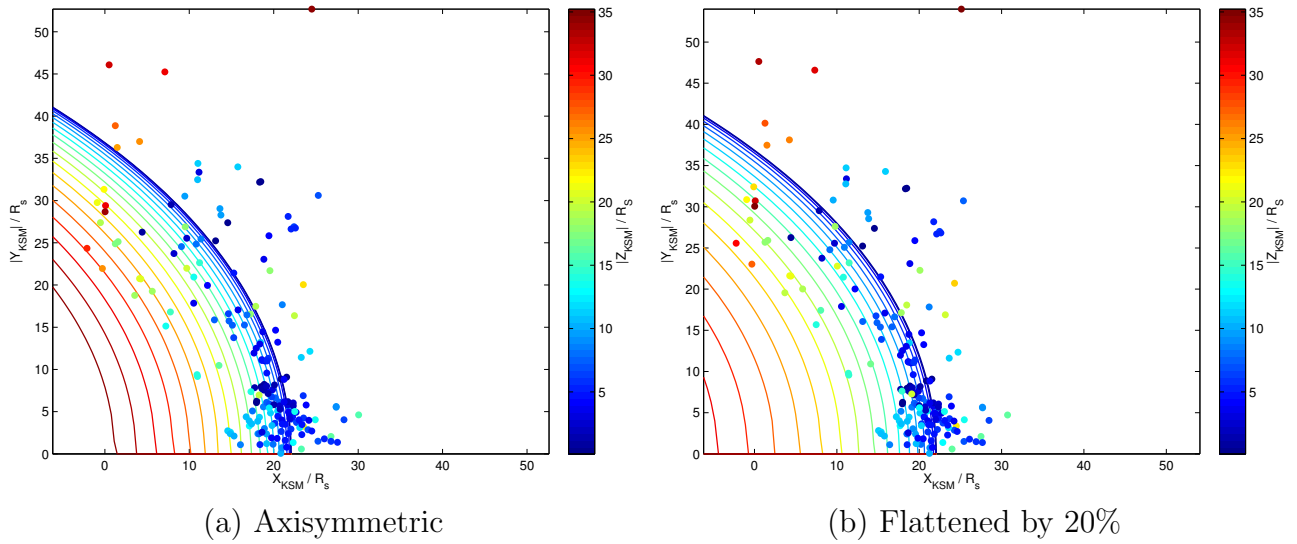


Figure 3. Magnetopause crossing locations are scaled to the average solar wind dynamic pressure and are coloured by their Z_{KSM} coordinate. On top of this has been plotted an X-Y slice every $2 R_S$ from (a) the axisymmetric model of *Kanani et al.* [2010] and (b) a flattened version of this model with a value of \mathcal{E} of 0.80.

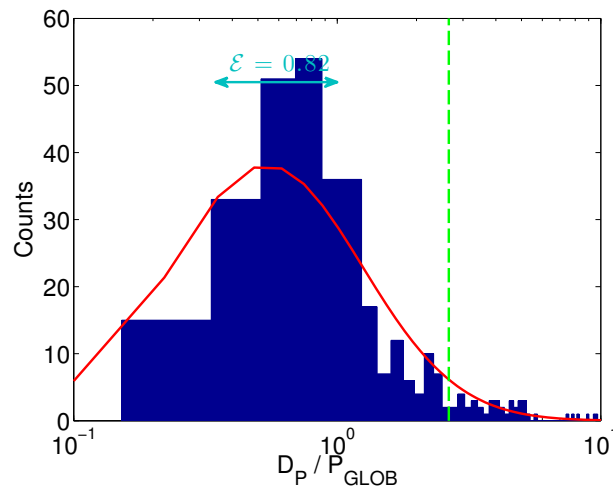


Figure 4. The ratio of the pressure estimate found assuming pressure balance and the pressure estimate found by fitting the *Kanani et al.* [2010] model through each crossing location has been calculated. This histogram shows the distribution of these ratios on a logarithmic axis and on top of this is plotted a log-normal curve (red line). The arrowed line indicates the range of ratios expected if an axisymmetric model is fitted through the surface of a flattened magnetopause model.

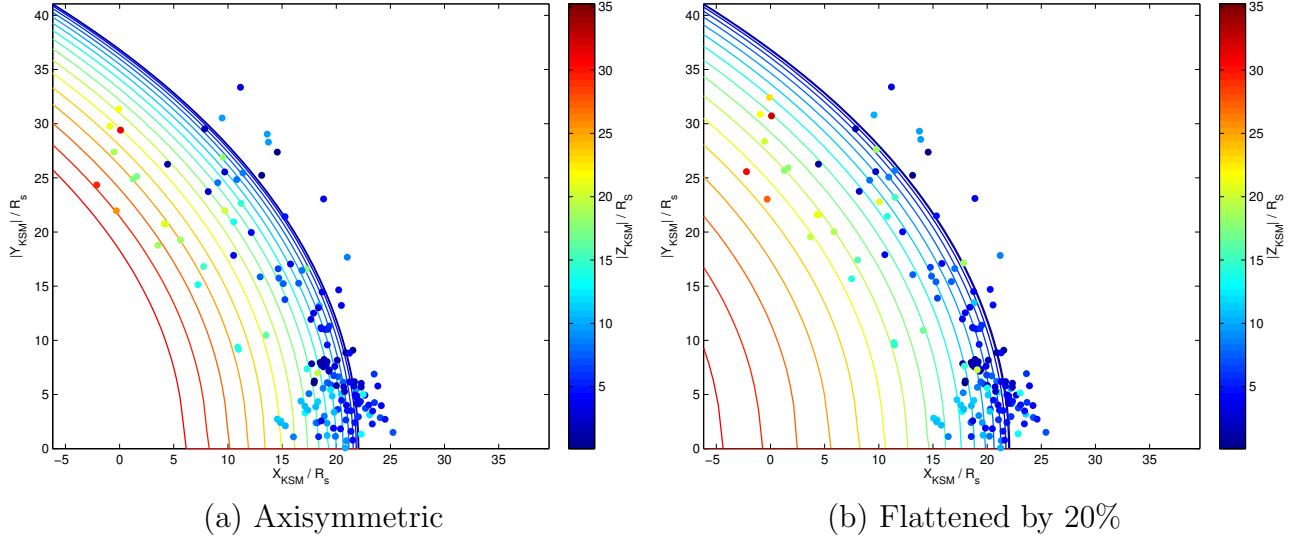


Figure 5. Magnetopause crossing locations are scaled to the average solar wind dynamic pressure and are coloured by their Z_{KSM} coordinate. On top of this has been plotted X-Y slices every $2 R_S$ from (a) the axisymmetric model by *Kanani et al.* [2010] and (b) a flattened version of this model with a value of \mathcal{E} of 0.80. The data is filtered based on the pressure ratio shown in Figure 4 to show crossings where the magnetopause can be assumed to be in equilibrium.

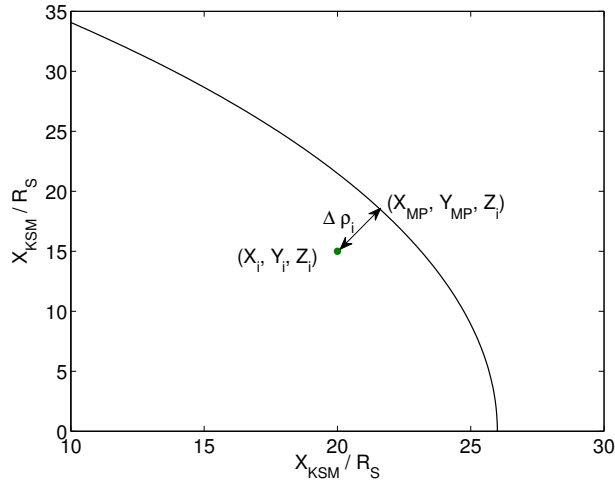


Figure 6. Illustrated is the distance $\Delta\rho_i$, the distance between a normalised magnetopause crossing and an X-Y slice (at the Z_{KSM} coordinate of the crossing) from a magnetopause surface constructed at $\langle D_P \rangle$. $\langle D_P \rangle$ is the pressure to which the crossings are normalised.

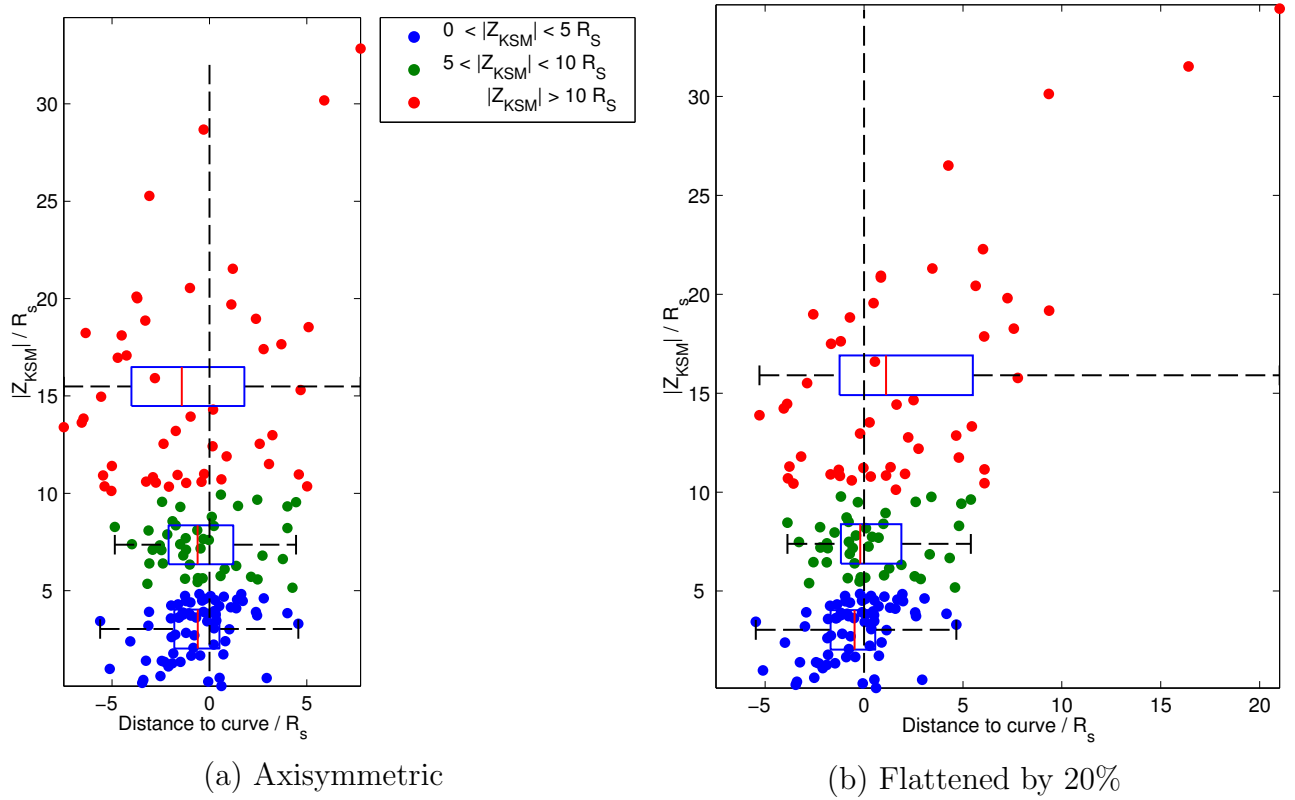


Figure 7. Plotted is the distance between the normalised X-Y position of each crossing and the X-Y slice plotted at the Z_{KSM} coordinate of each crossing from (a) the axisymmetric model of *Kanani et al.* [2010] and (b) a flattened version of this model with a value of \mathcal{E} of 0.80. The distance has been defined such that if a crossing is above (below) the magnetopause the distance is positive (negative). The crossings have been arbitrarily separated into bands of Z_{KSM} at $5 R_S$ intervals, but the minimum number of crossings within each band has been kept at 25 by collapsing the bands at large Z_{KSM} . Adjusting the width of these bands has little effect on the results of the statistics shown in Table 1. A box plot has been plotted on top of this for each band. The reduced data set has been used.

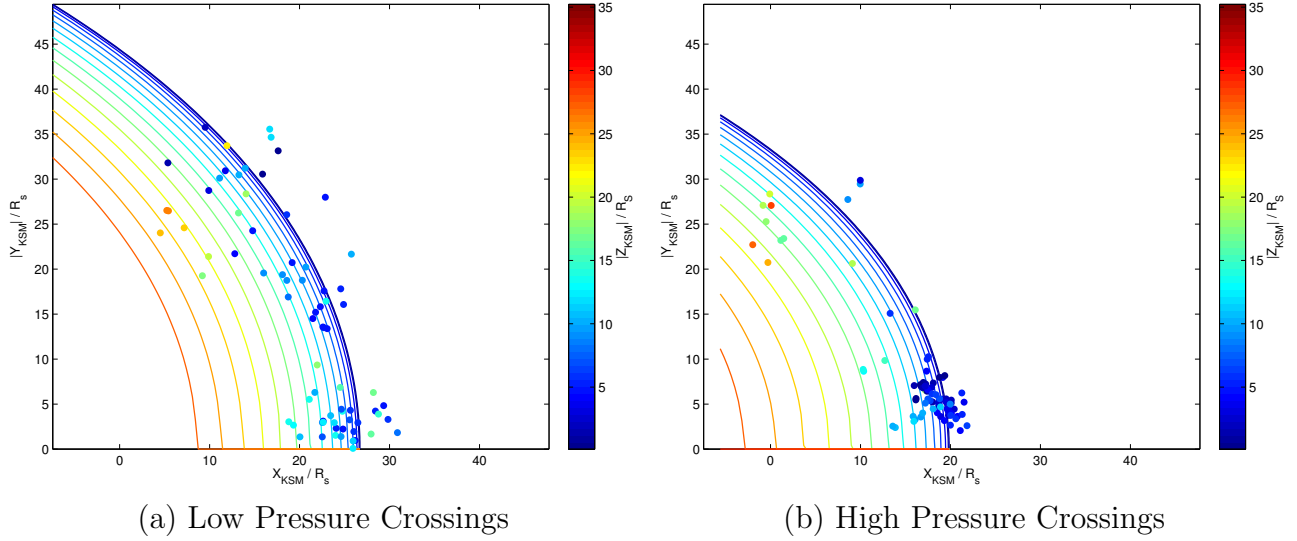


Figure 8. The crossings have been split into two populations, (a) one of lower than average dynamic pressure and (b) one of higher than average dynamic pressure. X-Y slices of a model flattened using a value of \mathcal{E} of 0.81 have then been plotted over the crossing positions.

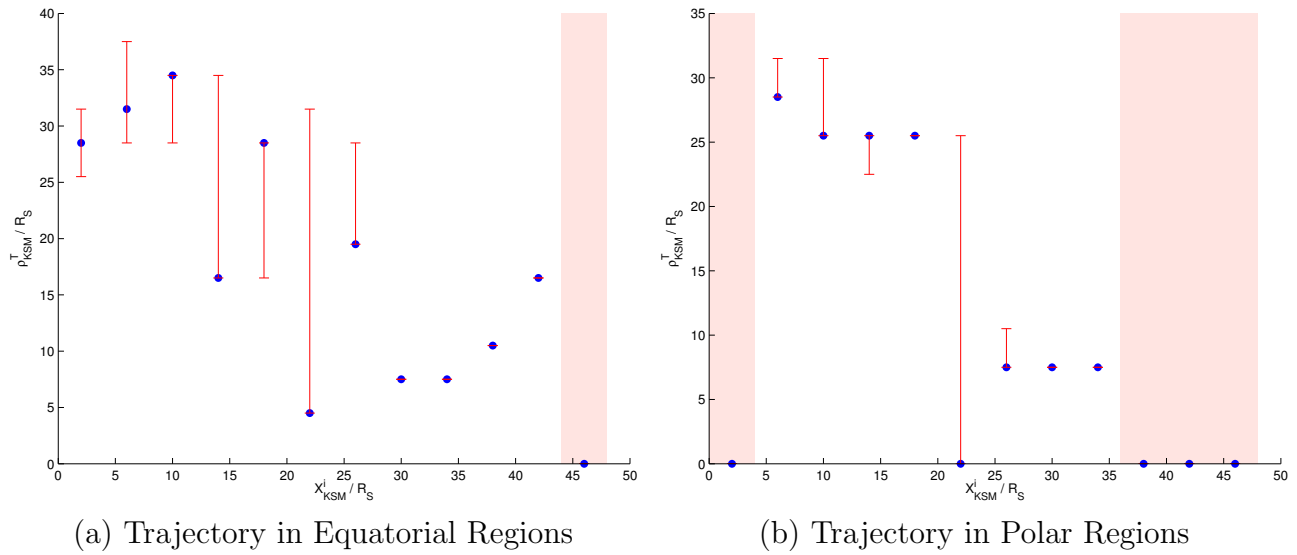


Figure 9. The ‘transition distance’, ρ_{KSM}^T , has been determined through analysis of the spacecraft trajectories over which the magnetopause crossings used in this study were found, and is plotted for each X_{KSM}^i bin as blue points. Regions where a transition distance could not be identified are shaded red. Confidence intervals are also included and were determined using Monte Carlo Bootstrap simulations resampling 1000 times for each X_{KSM}^i bin.

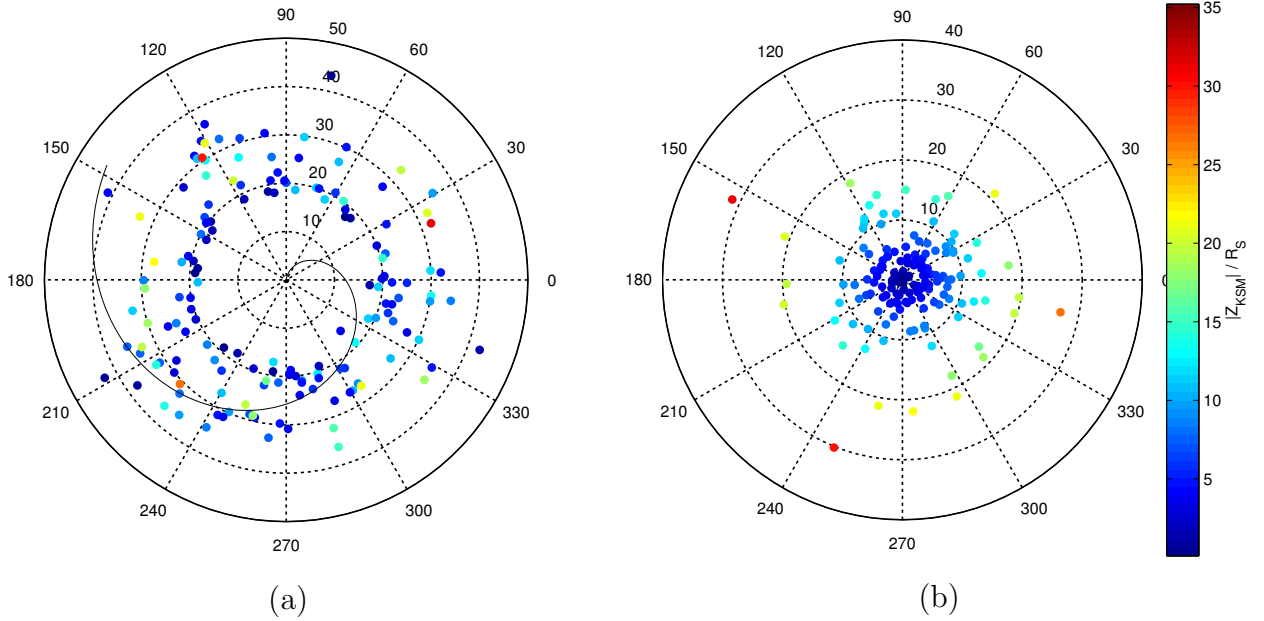


Figure 10. The reduced set of magnetopause crossings have been transformed into the SLS3 longitude system of *Kurth et al.* [2008]. In (a) the crossings are plotted in this system, the radial distance corresponds to the planet-crossing distance and the crossings are coloured by their normalised Z_{KSM} coordinates for comparison with other figures. The peak phase front is plotted as a dark line. In (b) the phase difference between each magnetopause crossing and the peak phase front is plotted in order to account for the effects of the bend back of the phase front due to the finite wave speed. The markers surrounding the outermost circle denote the phase difference and the inner markers denote the Z_{KSM} coordinate of each crossing. There is good coverage of crossings at large Z_{KSM} (coloured green-red).